P Cahyna et al.

Evaluation of first wall heat fluxes due to magnetic perturbations for a range of ITER scenarios

Evaluation of first wall heat fluxes due to magnetic perturbations for a range of ITER scenarios

P. Cahyna[a*], L. Kripner[a,b], A. Loarte[c], G. Huijsmans[c], M. Peterka[a,b], R. Panek[a]

[a]*Institute of Plasma Physics ASCR, Prague, Czech Republic*

[b]*Charles University in Prague, Faculty of Mathematics and Physics*

[c]*ITER Organization, Route de Vinon-sur-Verdon, CS 90 046, 13067 St. Paul Lez Durance Cedex, France*

Abstract The proposed use of magnetic perturbations for edge-localized mode (ELM) control in ITER poses a number of integration issues, among them the localized heat fluxes (footprints) on the plasma-facing components (PFCs). They may provide the benefit of spreading the heat flux, thus reducing its peak value, but they may cause a localized erosion of the PFCs. We present calculations of heat fluxes for a range of ITER plasma parameters. The efficiency of our method enables us to perform calculations for a range of assumptions on the SOL width and to optimize the coil configuration to yield the largest power flux spreading. The optimal coil configuration is not sensitive on SOL parameters and is also close to the one which is considered optimal for ELM control. The proximity of footprints may cause significant power loads on the upper wall.

1 Introduction

Resonant magnetic perturbations (RMPs) imposed by coils are one of the two methods of edge localized mode (ELM) control considered in the ITER Baseline [1]. ELM control is required because of the expected ELM energy loss, which for the ITER baseline (15 MA) scenario is at least 10 times larger than the size for an acceptable erosion lifetime of ITER PFCs, as well as for tungsten accumulation control [2]. While the RMPs produced by the ITER ELM control coils have the potential of suppressing or mitigating the ELMs, their application can have other side effects. One of them is the formation of spiralling flux footprints on the divertor [3]. This may lead to integration issues that need to be quantified in ITER, namely:

- possible non-axisymmetric erosion and re-deposition of the divertor material,

- localized non-toroidally symmetric power fluxes away from the separatrix that can potentially be larger than at the separatrix itself (where the divertor plasma is semi-detached in ITER) if the plasma in the footprints is attached,

- increased power fluxes to some regions of the first wall which is made of beryllium in ITER (particularly at the top of the device due to the proximity of the secondary X-point) and has lower power handling capability than the divertor target.

If non-axisymmetric erosion and localized peaks of heat flux on the divertor are indeed a real problem for ITER, their impact may be mitigated by a continuous rotation of the perturbation field by time-varying currents in the coils [2]. The rotation of the field will lead to a corresponding rotation of the footprint pattern, causing a beneficial toroidal spreading of the thermal load, erosion and redeposition. This is feasible thanks to the foreseen independent power supplies for each of the 27 ELM control coils. This solution has however a drawback of increasing the mechanical stress on the coils due to cyclical electromagnetic loads. Evaluation of the need for rotating RMP fields and the required frequency is therefore desirable (lower frequency being preferred as it leads to fewer

electromagnetic load cycles).

The power and particle fluxes in the footprints in ITER for attached divertor plasma conditions have been the subject of previous studies with the EMC3-EIRENE code (e.g. [4]), but only a few cases could be modelled due to the complexity of the 3-D transport modelling required. The results are therefore not suitable for a systematic optimization of the coil configuration. Such an optimization would require a large number of simulations due to the large parameter space of coil configurations (in principle 27 dimensions). In addition the details of scrape-off layer transport in ITER, in particular the form of the power decay function, are not known with certainity [5] and thus a range of assumptions should be included in the simulations. With a full-tungsten divertor, ELM mitigation is required in order to control tungsten accumulation in plasma even for low current scenaria where the ELM heat loads themselves would be otherwise tolerable [2]. ELM mitigation is also required during the plasma current ramp-up and ramp-down [6]. Those considerations mean that the optimization of coil configuration need to be performed for a range of operating scenaria and scrape-off layer characteristics, thus further multiplying the number of simulations needed. A very efficient method for the estimation of the power flux distribution in the footprints is thus required. We described such a method based mostly on analytic calculations in [7] and we benchmarked it against EMC3-EIRENE results for DIII-D.

In this paper we describe the results of applying the method to ITER, exploiting its efficiency in order to perform calculations for a wide range of conditions. Our task is analogous to the optimization procedure described in [6], where the performance of the ITER ELM control coils for a range of operating scenaria was evaluated. The performance metric was chosen as the width of the overlap region of vacuum field islands and evaluated in a high resolution scan of the parameter space. In our paper we use a similar procedure. In addition in [6] the footprints for a subset of the parameter space were calculated by field line tracing. Our work can be thought of as a continuation where we calculate the footprints for the whole parameter space and we perform an estimation of the power

fluxes instead of just calculating the magnetic topology. In particular we calculate the power flux to the upper wall panels.

A crucial decision is the choice of the metric for optimization. There are several possibilities: one may want to search for a configuration with the shortest footprints in order to have the most symmetric loads. In this case the impact of footprints on surfaces not designed to handle high power loads will be also minimized. This used to be the issue with the combined CFC/tungsten divertor design for the non-active phase, where a long footprint spiral could have extended from the strike point target made of CFC into the area made from tungsten. Keeping the footprints short would therefore enhance the operational flexibility in the non-active phase, as tungsten melting would not be an issue and higher heat fluxes could be tolerated. Since then the ITER strategy shifted to a full tungsten divertor even in the non-active phase [8]. Whether keeping the footprints short brings an advantage therefore depends on the power handling capability of different areas of the divertor (baffle vs. vertical targets).

An opposite strategy is to search for largest power spreading. As the total power is fixed, if it is being spread to a larger area, the peak flux decreases. One may intuitively expect the spreading to be corelated with footprint length. Therefore the power flux will have a more toroidally asymmetric distribution, but its amplitude will be smaller and thus the asymmetry will be less of an issue. Discussion of how a decrease of peak heat flux in the footprints leads to a lower requirement for the rotation frequency of the perturbation can be found in [2]. The power spreading is the metric that we chose in this work. (Note that a related metric of footprint area was chosen in [6].) It is still an issue if the footprints are so long that they touch the upper part of the wall where there is no divertor but only beryllium panels with a lower power handling capability. This might happen due to the strong shaping of the ITER plasma which has the upper X-point fairly close to the plasma boundary. It is known that close to a double-null configuration the homoclinic tangle may undergo a bifurcation and the footprints may start touching the upper wall panels [9]. The ITER Quasi-double-null (QDN) scenario can be expected to

be the most susceptible to this bifurcation.

In this paper we therefore use the following strategy: we calculate the coil configuration with the maximum power flux spreading for every combination of assumptions on the SOL transport. For the upper wall we find the maximum heat flux across all the configurations and assumptions on the SOL transport in order to know the worst case.

2 Methods

For the calculation of the perturbed heat flux we use the tangle distance method described in [7]. The power flux density $q_\parallel$ in the SOL is supposed to have the form $q_\parallel(\Delta r) = q_{\text{sep}} f(\Delta r)$ where Δr is the distance from the separatrix at the midplane, which in the presence of the magnetic perturbation is replaced by the tangle distance (the distance to the outermost manifold of the homoclinic tangle).

In [7] the power decay in the SOL was considered to be exponential: $f(\Delta r) = \exp(-\Delta r/\lambda_{\text{sep}})$. Experimentally the SOL power flux profile in H-mode is found to have two decay lengths: one near the separatrix which is very narrow and one that extended further from the separatrix in the SOL which is rather broad. The one near the separatrix is found to scale with plasma current and is most likely related to ion neoclassical transport [10] while the one far from the SOL is related to turbulent or blobby transport bringing particle and convective heat to the wall. Here we therefore consider a double exponential profile with a narrow SOL near the separatrix (λ_{sep}) and a far-SOL ($\lambda_{\text{far-SOL}}$). These two values are required to evaluate the effect of the heat flux splitting both on the divertor and wall power fluxes. The values chosen in this article cover the range expected in ITER for 15 MA operation with $Q \approx 10$ from 2-5 mm for the near SOL (see [5]) and 40 to 170 mm for the far SOL (see [11]). It is assumed that the narrow scale length dominates the power profile near the separatrix for distance up to $\alpha\lambda_{\text{sep}}$, where α is typically between 1 and 2.

In [7] the resulting function was supposed to represent the perpendicular heat flux $q_\perp$

to the divertor surface. The flux expansion factor, being assumed to be constant in the region of interest, was contained together with q_{sep} in the constant multiplier q_0 in front of the exponential. Here we calculate the heat flux on a large area of the divertor and wall, where the flux expansion varies considerably, so we can not make this assumption and we multiply $q_{\parallel}$ by the local flux expansion factor in order to yield $q_{\perp}$. The wall panels are roof-shaped in the toroidal direction, which increases the incident angle of field lines. In this work we approximate this effect by a constant 7° toroidal inclination of the wall surface. The values of the angle field line on the region of the upper wall in ITER are dominated by their toroidal inclination angle which is $\approx 5°$ (see [12]); the contribution of the field line angle itself to the variation of the angle is small because the plasma configurations in ITER have a secondary X-point near the upper part of the wall. A 2° angle has been chosen as an upper limit for the field line impact angle leading to an effective 7° impact angle. In fact the real angles in the region of highest power loads near the top of the device (closest to the secondary X-point) are lower than that because the poloidal field is low there.

Finally, as noted in [7], the total power flux across the separatrix is constant, thus $q_{\perp}$ needs to be normalized in order to keep its integral over the whole tokamak wall the same as for the heat flux $q_{\perp,\text{unpt}}$ in the unperturbed case: $\int q_{\perp}\mathrm{d}S = \int q_{\perp,\text{unpt}}\mathrm{d}S$. We achieve this by calculating the heat flux $q_{\perp,0}$ without the normalization and dividing it by the factor $A = \int q_{\perp,0}\mathrm{d}S / \int q_{\perp,\text{unpt}}\mathrm{d}S$ which we call the power spreading factor. In presence of perturbations $A > 1$ as the footprints open new transport channels for the heat flux. Larger spreading factor leads to more significant reduction of heat flux peaks. We thus optimize the coil configuration in order to yield the largest possible spreading factor.

The calculations were performed for all the combination of the following values of the SOL parameters: $\alpha \in \{1, 2\}$, $\lambda_{\text{sep}} \in \{2\,\text{mm}, 5\,\text{mm}\}$, $\lambda_{\text{far-SOL}} \in \{40\,\text{mm}, 170\,\text{mm}\}$.

In order to perform the optimization we need to have a fast method of evaluation of the tangle distance function. We use the Melnikov integral approximation as detailed in [7]. For the application to ITER it is important that it is a first order, linear approximation.

The total Melnikov integral M of a coil configuration is a sum of Melnikov integrals for the individual coils and the Melnikov integral for i-th coil can be calculated just for a unit current of 1 kAt (we note it M_i) and multiplied by the coil current I_i in kAt. The total Melnikov integral is the linear combination $M = \sum_{i=1}^{27} I_i M_i$. Once the basis M_i is calculated for a given equilibrium, calculating the total M for a given coil configuration is very efficient.

The coil configuration space was reduced to two dimensions using the upper and lower row phase angles $\Delta\phi_U$ and $\Delta\phi_L$ respectively, for a $n = 3$ perturbation symmetry and peak current $I_c = 90$kAt. Formula given in [6] yields the currents I_i as functions of $\Delta\phi_U, \Delta\phi_L$.

3 Results

We analyzed the ITER 15 MA H-mode quasi-double-null scenario with $T_e = 4.5\,\text{keV}$. The Melnikov integral method allows us to calculate the length of the magnetic footprints (the maximum displacement of the stable or unstable invariant manifold). This value depends only on the magnetic configuration, not on the SOL parameters. The result mapped to the midplane is shown in Fig. 1 for both the inner and outer divertor footprints. The inner divertor footprints also determine the loads on the upper wall panel because the separatrix lobes at the top of the plasma and at the inner divertor are formed by the same invariant manifold. We may see that the results are quite different for the inner and outer footprints and the inner footprints show secondary local maxima in addition to the global maximum near the center of the image, as well as secondary local minima.

For all eight combination of the SOL parameters α, λ_{sep}, $\lambda_{\text{far-SOL}}$ we then found the combination of phase angles which yields the largest power flux spreading A (the best attainable spreading that can be obtained by adjusting coil currents). The results are summarized in Table 1. For the case where the maximum attainable A is the smallest among the SOL parameters we show the dependency $A(\Delta\phi_U, \Delta\phi_L)$ in Fig. 2. It has a form of a single smooth peak, with the maximum located near the maximum length of

the inner footprints. The power flux spreading factor never drops below 1.

In Table 2 we show the maximum heat flux in the perturbed (coils on) case on the upper wall among all the combinations of the SOL parameters and phase angles, thus the worst case possible in our model. The maximum heat fluxes for the axisymmetric (coils off) case with the same parameters are calculated by the same method for comparison. The dependence of the maximum on phase angles $\Delta\phi_U$, $\Delta\phi_L$ for constant values of SOL parameters is shown in Fig. 3. The maximum heat flux is determined by both the footprint length (Fig. 1) and the spreading factor (Fig. 2) whose effect is opposite: peak heat flux shall increase with footprint length and decrease with spreading. We indeed see that it has a similar dependency as the footprint length, but with the secondary maxima comparable to the primary one. The reason is that the primary maximum coincides with the maximal flux spreading, which acts to reduce the peak flux.

4   Discussion and conclusion

The graphs of the footprint length as a function of the phase angles look very similar to the graphs of the vacuum island overlap width parameter (Δ_{VIOW}) in [6]. The reason is probably that the resonant components of the perturbation field, which determine the island sizes and thus the overlap width, are given by the same Melnikov integral-type expression as the length of the footprints [13] which for the vacuum field of the coils is usually strongly correlated at the separatrix (where it determines the footprints) and inside the plasma (where it determines the island sizes) [14]. The maximum power flux spreading by footprints is also achieved for similar values of the phase angles as the maximum footprint length, which is expected as the footprints are responsible for the spreading. The angles which yield the maximum spreading are only weakly sensitive on the assumptions on the scrape-off layer width, but the absolute value of the maximal spreading strongly depends on them, the minimum (the worst case) being reached for the narrowest SOL.

The footprints never touch the upper wall — the bifurcation described in [9] does not happen even for the QDN case, which is still too far from a true double-null configuration. The proximity of the footprints to the upper wall still produces peaks of heat flux there due to the deformation of the SOL around the footprints. The maximum value of heat flux on the upper wall is in some cases being reached for the same phase angles as the longest inner footprints, as longer footprints are closer to the wall. This effect may be compensated by the power spreading, which decreases the flux and thus reduces the peaks. In other cases the maximum heat flux is therefore reached for very different combinations of the phase angles and the peaks may be even smaller than the peak heat flux for the unperturbed case.

The choice of λ and α in our study is done to provide an upper limit of the loads to the upper wall and, in an average way, include the effects of ELMs. Because of this we get heat loads on the upper wall close to the handling limit of 4.7 MW/m^2 in the axisymmetric situation in QDN, which is the design condition for these upper first wall panels. This leads to heat loads exceeding the handling limit in the quasi-stationary situation for some choices of phases for the coil currents when 3-D fields are applied. The choice of coil phasing may therefore be important. So far we have used the power spreading as the value to maximize, but we did not concern ourselves with the efficiency of the ELM control coils for their primary purpose — ELM control. As we have found, the power flux correlates with the vacuum island overlap width, so a configuration optimal from the point of view of spreading the power flux will likely have a good performance for ELM control. Nevertheless, we have seen that this is unfortunately also the configuration with the longest footprints and in some cases may lead to power fluxes larger than the design value of the upper wall. This is an important issue which should be clarified using a more detailed study, namely by using the true three-dimensional shape of the first wall panels instead of the simplified constant inclination which we have used here. It may turn out that choosing particular values of phase angles will be required for some SOL parameters in order to satisfy the loading limit. In this case we should perform

a combined optimization procedure which will keep a predetermined value of Δ_{VIOW}. If the stationary heat fluxes are found to be incompatible with good ELM control, the perturbation field will need to be rotated as foreseen [2] or the QDN scenario will need to be avoided.

One factor not considered in this study is the plasma response. The loads on the upper wall would still increase if the global MHD response of the plasma distorts the boundary and causes it to locally approach the wall [15]. Our calculation otherwise represent an upper bound of the heat fluxes: screening of perturbation by plasma is expected to reduce the footprint length [16, 4, 17] and therefore the loads on the upper wall. Only the spreading factor may be overestimated as screening by plasma will likely reduce it.

In summary, we have a very efficient method to evaluate and optimize the power fluxes for various configurations of ITER and we found that some cases may lead to power fluxes larger than the design value of the upper wall, which could restrict operation with RMPs and warrants a more detailed study with a more realistic model of the wall. Using the efficiency of the method, more cases should be studied. Among them are other equilibria and the $n = 4$ and failure cases of the ELM control coils. It could be said that the difficulty shifts from the calculation of the fluxes to the choice of the metric for optimization. The choice of the metric is especially important for the $n = 4$ configuration, where the footprints are less symmetric and one will need to find a well symmetric configuration, otherwise the requirements on the frequency of the perturbation rotation will increase [2].

5   Acknowledgements

expressed herein do not necessarily reflect those of the European Commission.

The views and opinions expressed herein do not necessarily reflect those of the ITER Organization.

References

[1] T. Evans, Journal of Nuclear Materials **438, Supplement** (2013) S11 – S18.

[2] A. Loarte, et al., Nuclear Fusion **54** (2014) 033007.

[3] T. E. Evans, et al., Journal of Physics: Conference Series **7** (2005) 174–190.

[4] O. Schmitz, et al., Journal of Nuclear Materials **438, Supplement** (2013) S194 – S198.

[5] A. Kukushkin, et al., Journal of Nuclear Materials **438, Supplement** (2013) S203–S207.

[6] T. Evans, et al., Nuclear Fusion **53** (2013) 093029.

[7] P. Cahyna, et al., Nuclear Fusion **54** (2014) 064002.

[8] T. Hirai, et al., Fusion Engineering and Design **88** (2013) 1798 – 1801, proceedings of the 27th Symposium On Fusion Technology (SOFT-27); Lige, Belgium, September 24-28, 2012.

[9] R. K. W. Roeder, et al., Physics of Plasmas **10** (2003) 3796–3799.

[10] T. Eich, et al., Nuclear Fusion **53** (2013) 093031.

[11] A. Loarte, et al., in *Fusion Energy 2008 (Proc. 22nd Int. Conf. Geneva)*, (Vienna: IAEA), 2008 CD-ROM file IT/P6-13 and http://www-naweb.iaea.org/napc/physics/FEC/FEC2008/html/index.htm.

[12] R. Mitteau, et al., Journal of Nuclear Materials **415** (2011) S969 – S972, proceedings of the 19th International Conference on Plasma-Surface Interactions in Controlled Fusion.

[13] I. Joseph, et al., Nuclear Fusion **48** (2008) 045009.

[14] P. Cahyna, E. Nardon, *Resonant magnetic perturbations and divertor footprints in poloidally diverted tokamaks* (2010), `arXiv:1005.3663 [physics.plasm-ph]`.

[15] I. T. Chapman, et al., Plasma Physics and Controlled Fusion **54** (2012) 105013.

[16] P. Cahyna, et al., Journal of Nuclear Materials **415** (2011) S927–S931, `arXiv:1012.4015 [physics.plasm-ph]`.

[17] F. Orain, et al., Physics of Plasmas **20** (2013) 102510.

Tables

$\lambda_{\text{sep}}/\lambda_{\text{far-SOL}}$ [mm]	α	$\Delta\phi_U/\Delta\phi_L$ [Deg.]	max A
2/40	2	66/56	2.63
5/40	2	65/56	2.17
2/40	1	66/56	1.68
2/170	2	66/56	1.62
5/40	1	65/56	1.60
5/170	2	66/56	1.53
2/170	1	66/56	1.18
5/170	1	65/56	1.17

Table 1: Maximum spreading factor A and the position of the maximum in the $\Delta\phi_U/\Delta\phi_L$ space for every combination of SOL parameters.

$\lambda_{\text{sep}}/\lambda_{\text{far-SOL}}$ [mm]	α	$\Delta\phi_U/\Delta\phi_L$ [Deg.]	max heat flux [MW/m^2]:	
			perturbed	axisymmetric
2/170	1	15/18	3.70	3.45
2/170	2	23/107	3.14	3.31
2/40	1	56/65	7.58	4.66
2/40	2	15/18	4.80	4.04
5/170	1	15/18	3.68	3.41
5/170	2	24/108	2.99	3.10
5/40	1	57/64	8.19	4.49
5/40	2	16/19	4.68	3.44

Table 2: Maximum heat flux on the upper wall, values of phase angles at the maximum and the maxima for the corresponding axisymmetric cases.

Figure captions

Figure 1: Maximum length of the inner (left) and outer (right) footprints mapped to the outboard midplane as a function of the phase angles.

Figure 2: Dependence of the spreading factor A on phase angles $\Delta\phi_U$, $\Delta\phi_L$, $\alpha = 1$, $\lambda_{\text{sep}} = 5$ mm, $\lambda_{\text{far-SOL}} = 170$ mm.

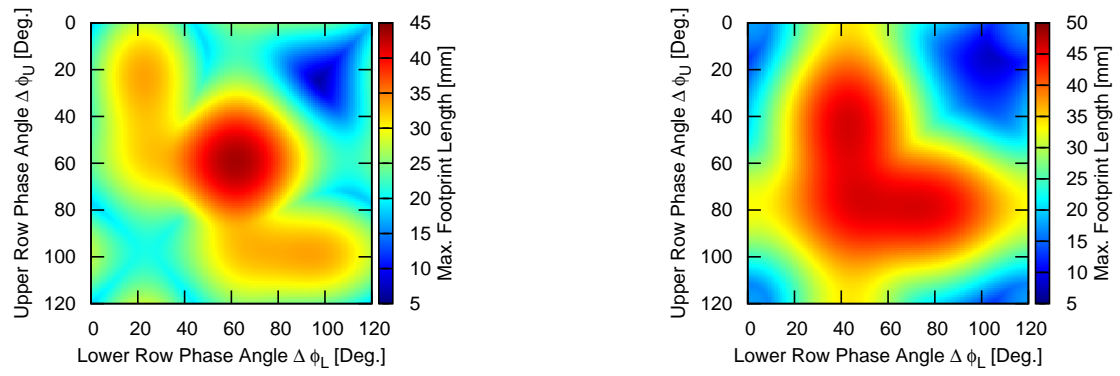Figure 3: Maximum heat flux on the upper wall as a function of the phase angles.
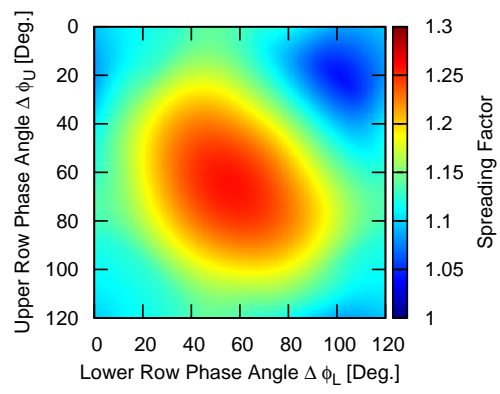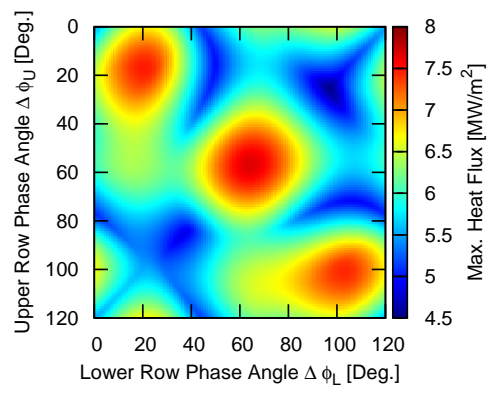
Figures

Fig. 1

Fig. 2

Fig. 3